


# Measurement of $^{232}$Th (n, $\gamma$) cross section at the CSNS Back-n facility in the unresolved resonance region from 4 keV to 100 keV

Bing Jiang(姜炳), Jianlong Han(韩建龙), Jie Ren(任杰), Wei Jiang(蒋伟), Xiaohe Wang(王小鹤), Zian Guo(郭子安), Jianglin Zhang(张江林), Jifeng Hu(胡继峰), Jingen Chen(陈金根), Xiangzhou Cai(蔡翔舟), Hongwei Wang(王宏伟), Longxiang Liu(刘龙祥), Xinxiang Li(李鑫祥), Xinrong Hu(胡新荣), and Yue Zhang(张岳)

**Citation:**Chin. Phys. B, 2022, 31 (**6**): 060101. DOI: 10.1088/1674-1056/ac5394
Journal homepage: http://cpb.iphy.ac.cn; http://iopscience.iop.org/cpb

**What follows is a list of articles you may be interested in**

---

## Detailed calibration of the PI-LCX: 1300 high performance single photon counting hard x-ray CCD camera

Wei Hong(洪伟), Xian-Lun Wen(温贤伦), Lai Wei(魏来), Bin Zhu(朱斌), Yu-Chi Wu(吴玉迟), Ke-Gong Dong(董克攻), Chun-Ye Jiao(焦春晔), Bo Wu(伍波), Ying-Ling He(何颖玲), Fa-Qiang Zhang(张发强), Wei-Min Zhou(周维民), Yu-Qiu Gu(谷渝秋)

Chin. Phys. B, 2017, 26 (**2**): 025204. DOI: 10.1088/1674-1056/26/2/025204

## Spectral and ion emission features of laser-produced Sn and $SnO_2$ plasmas

Hui Lan(兰慧), Xin-Bing Wang(王新兵), Du-Luo Zuo(左都罗)

Chin. Phys. B, 2016, 25 (**3**): 035202. DOI: 10.1088/1674-1056/25/3/035202

## Simulations of the L–H transition dynamics with different heat and particle sources

Li Hui-Dong, Wang Zhan-Hui, Jan Weiland, Feng Hao, Sun Wei-Guo

Chin. Phys. B, 2015, 24 (**11**): 115204. DOI: 10.1088/1674-1056/24/11/115204

## Compound sawtooth in EAST LHCD plasma： An experimental study

Xu Li-Qing, Hu Li-Qun, Chen Kai-Yun, Li Miao-Hui

Chin. Phys. B, 2014, 23 (**8**): 085201. DOI: 10.1088/1674-1056/23/8/085201

## Ray tracing method for the grazing incidence flat-field imaging soft X-ray spectrometer

Dong Quan-Li, Liu Yun-Quan, Teng Hao, Li Ying-Jun, Zhang Jie

Chin. Phys. B, 2014, 23 (**6**): 065206. DOI: 10.1088/1674-1056/23/6/065206

---

**DATA PAPER**

# Measurement of $^{232}$Th $(n,\gamma)$ cross section at the CSNS Back-n facility in the unresolved resonance region from 4 keV to 100 keV

Bing Jiang(姜炳)[1,2,3], Jianlong Han(韩建龙)[1,2,3], Jie Ren(任杰)[4], Wei Jiang(蒋伟)[5,6], Xiaohe Wang(王小鹤)[1,2,†], Zian Guo(郭子安)[1,2,3], Jianglin Zhang(张江林)[1,2,3], Jifeng Hu(胡继峰)[1,2], Jingen Chen(陈金根)[1,2,3,‡], Xiangzhou Cai(蔡翔舟)[1,2,3,§], Hongwei Wang(王宏伟)[3,7], Longxiang Liu(刘龙祥)[7], Xinxiang Li(李鑫祥)[1,3], Xinrong Hu(胡新荣)[1,3], and Yue Zhang(张岳)[5,6]

[1] *Shanghai Institute of Applied Physics, Chinese Academy of Sciences, Shanghai* 201800, *China*
[2] *CAS Innovative Academy in TMSR Energy System, Chinese Academy of Sciences, Shanghai* 201800, *China*
[3] *University of Chinese Academy of Sciences, Beijing* 100049, *China*
[4] *Key Laboratory of Nuclear Data, China Institute of Atomic Energy, Beijing* 102413, *China*
[5] *Institute of High Energy Physics, Chinese Academy of Sciences, Beijing* 100049, *China*
[6] *China Spallation Neutron Source, Dongguan* 523803, *China*
[7] *Shanghai Advanced Research Institute, Chinese Academy of Sciences, Shanghai* 201210, *China*

(Received 11 November 2021; revised manuscript received 11 January 2022; accepted manuscript online 10 February 2022)

The neutron capture cross section of $^{232}$Th was measured at the neutron time-of-flight facility Back-n of China Spallation Neutron Source (CSNS) for the first time. The measurement was performed with 4 hydrogen-free deuterated benzene $C_6D_6$ liquid scintillation detectors, in the ES#2 experiment station on the beam line, at a distance of about 76 m from the neutron-production assembly. The total energy detection principle in combination with the pulse height weighting technique (PHWT) was applied to analyze the measured data. Results of the $^{232}$Th $(n,\gamma)$ reaction cross section in the unresolved resonance region from 4 keV to 100 keV were obtained, which shows a good agreement with the existing experimental data from EXFOR, as well as with the evaluated data from the ENDF/B-VIII.0 and CENDL-3.1. In addition, the excitation function of $^{232}$Th $(n,\gamma)^{233}$Th reaction in the unresolved resonance region was theoretically calculated by using the code TALYS-1.95. By fitting the experimental cross section and theoretical data, the average parameters in the unresolved resonance region were extracted. The datasets are openly available at http://dx.doi.org/10.11922/sciencedb.j00113.00015.

**Keywords:** $^{232}$Th $(n,\gamma)$ cross section, CSNS Back-n facility, $C_6D_6$ detectors, unresolved resonance region

**PACS:** 01.52.+r, 24.30.–v, 29.25.Dz, 52.70.La **DOI:** 10.1088/1674-1056/ac5394

## 1. Introduction

Nowadays, the energy of nuclear fission has incomparable advantages in serving the ever growing requirements for energy and environmental protection. Compared to the traditional uranium–plutonium fuel cycle, the importance of thorium-based nuclear fuel has become increasingly prominent because of its excellent breeding capability in both thermal and fast reactors, lesser long-lived minor actinides resulting from fission, and abundant reserves of thorium.[1] Either the critical or the subcritical system based on Th–U fuel cycle becomes the focus of attention presently, such as the thorium molten salt reactor nuclear energy system (TMSR)[2] and the accelerator-driven sub-critical system (ADS).[3] The design and development of these innovation nuclear systems require precise neutron nuclear data of the key isotopes, since the simulation of the performances for these systems strongly depends on the cross sections of neutron-induced reactions. In this scenario, an accurate knowledge of the $^{232}$Th $(n,\gamma)$ cross section is of great importance in the thorium–uranium fuel cycle which is based on the fissile $^{233}$U formed by neutron-induced capture on the fertile $^{232}$Th.

The TMSR system is designed for thorium-based nuclear energy utilization and it is committed to achieving the comprehensive utilization of nuclear energy.[1,2] The use of thorium can significantly reduce the generation of high-level radioactive waste of spent fuel, which is an interesting advantage compared to the uranium fuel. For TMSR, $^{232}$Th is the 'beginning' nuclide of the thorium–uranium cycle chains, which makes the neutron capture data of $^{232}$Th an essential input for the critical performance and safe operation of the reactor core. In addition, a sensitivity analysis of nuclear data for the Th–U fuel cycle in the molten salt reactor shows that a 1% disturbance of the $^{232}$Th neutron capture cross sections would result in a 0.35% change of the $k_{\rm eff}$ for the core system,[4] which makes the accurate measurement of $^{232}$Th $(n,\gamma)$ cross section important for serving the neutron nuclear data requirements of the

†Corresponding author. E-mail: wangxiaohe@sinap.ac.cn
‡Corresponding author. E-mail: chenjingen@sinap.ac.cn
§Corresponding author. E-mail: caixiangzhou@sinap.ac.cn

© 2022 Chinese Physical Society and IOP Publishing Ltd 

TMSR system.

The available data of $^{232}$Th $(n,\gamma)$ cross section are mainly from evaluated nuclear data libraries or existing experimental data included in EXFOR. In recent years, several measurements of $^{232}$Th $(n,\gamma)$ cross section have been performed using the time-of-flight technique at different white neutron sources, e.g., n_TOF[5,6] and GELINA.[7,8] Although most of these experiments were carried out with high precision, the discrepancies of $^{232}$Th $(n,\gamma)$ cross sections still exist and cannot be ignored. The Back-n facility[9,10] is a newly built time-of-flight spectrometer at the China Spallation Neutron Source (CSNS),[11,12] which has been constructed with the aim of studying the neutron-induced reaction cross section for supporting the eminent demands for an enhanced nuclear database in China.[10] With a wide neutron energy spectrum, high neutron flux, and high time resolution of the Back-n facility, it motivates a $^{232}$Th $(n,\gamma)$ cross section experiment with high accuracy. No other work of the $^{232}$Th $(n,\gamma)$ cross section measurement has been performed at this facility before. The present work reports the data analysis procedure and the results of $^{232}$Th $(n,\gamma)$ cross section in the unresolved resonance region (URR) from 4 keV to 100 keV. The values of the experimental cross section are included in the supplementary materials (SM) in the form of excel files, which are openly available at http://dx.doi.org/10.11922/sciencedb.j00113.00015. Because the data analysis and the type of result presentation in the resolved resonance region (RRR) are significantly different from those in the URR, the results in the RRR will be described in detail in another literature to be published.

The rest of this paper is organized as follows. Section 2 provides a description of the experimental details. The data analysis procedure is described in Section 3. In Section 4, the results of experimental cross section are given and discussed. The excitation function of $^{232}$Th $(n,\gamma)^{233}$Th reaction calculated by using the theoretical code TALYS[13] is presented. In addition, the parameters used to describe the average cross section in the URR are also given in this section. The conclusions are presented in Section 5.

## 2. Experimental details

The measurement of $^{232}$Th $(n,\gamma)$ cross section has been performed at the Back-n time-of-flight facility of CSNS operated with the double-bunch mode. At Back-n, the primary neutrons are generated by spallation reactions induced by a 1.6 GeV/c proton beam impinging on a tantalum-cladded and water-cooled sliced tungsten target.[14] These primary neutrons are subsequently moderated by the spallation target itself and the surrounding moderators until they enter the evacuated neutron transport tube of the Back-n facility. Two experimental stations are located on the beam line at flight path lengths of approximately 55 m (ES#1) and 76 m (ES#2) from the spallation target. The present $^{232}$Th $(n,\gamma)$ measurement was performed at station ES#2, taking advantage of the low $\gamma$-rays background and excellent neutron energy resolution. A detailed description about the characteristics of the Back-n facility can be found elsewhere.[10,16] The Monte–Carlo calculation indicates that the time resolution is better than 1% at the experimental station which is located about 80 m away from the tungsten target in the energy range of 1 eV–1 MeV when the accelerator works in the single-bunch mode.[14,15] Therefore, the neutron energy can be accurately deduced by the time-of-flight technique.

A disk-shaped $^{232}$Th sample of 0.82 mm in thickness, corresponding to $1.819\times10^{-3}$ atoms/barn was used for the measurement. A natural carbon sample with the same diameter was used to evaluate the background resulting from sample scattered neutrons. In addition, a gold sample, as a standard isotope whose $(n,\gamma)$ cross section is well-known, was measured under the same condition to verify the data analysis procedure. The characteristics of the samples are listed in Table 1. Besides, an empty holder measurement was also carried out in order to estimate the background that is independent of the $^{232}$Th sample.

**Table 1.** Characteristics of samples.

| Sample | Shape | Diameter (mm) | Mass (mg) | Chemical form |
|---|---|---|---|---|
| $^{197}$Au | disk | 30 | 12680 | metal |
| $^{232}$Th | disk | 30 | 4953 | metal |
| $^{nat}$C | disk | 30 | 1300 | graphite |

The prompt $\gamma$-rays from the neutron capture of $^{232}$Th were detected with four hydrogen-free deuterated benzene $C_6D_6$ liquid scintillation detectors, which have been widely used for high resolution neutron capture cross-section measurements at the time-of-flight facilities by using the total energy detection principle in combination with the pulse height weighting technique (PHWT).[17–19] Figure 1 shows the $C_6D_6$ detector system which consists of four $C_6D_6$ detectors, one aluminum detector bracket and one sample holder. The type of the liquid scintillator in the $C_6D_6$ detectors is EJ315, and the aluminum shell wrapped around the scintillator is approximately 13 cm in diameter and 7.62 cm in thickness. In addition, an ETEL 9390KEB photomultiplier tube covered by an aluminum shell is directly mounted onto the scintillator. The four $C_6D_6$ detectors were installed at an angle of 110° relative to the direction of the neutron beam and about 15 cm (distance between the detector center and the sample center) upstream from the capture sample. Such experimental setup with backward angular of the detectors can sufficiently reduce the background resulting from scattered neutrons from the sample and the neutron beam dump.

The calibration of the $C_6D_6$ detector system was performed by measuring the response to three different radioactive sources of $^{137}$Cs (662 keV), $^{22}$Na (551 keV and 1274 keV)

and $^{238}$Pu/$^{13}$C (composite source, 6129 keV). Geant4 Monte–Carlo simulation together with experimental measurement of the deposited energy spectra of each source were performed for the detectors. The calibration results are reported in the literature.[20]

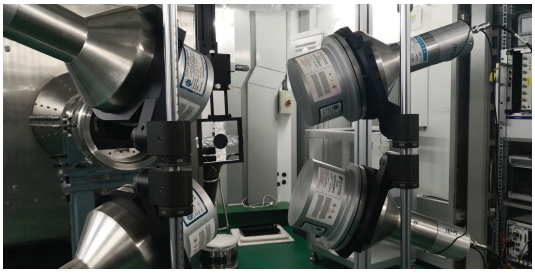


**Fig. 1.** $C_6D_6$ detector system at Back-n.

The data acquisition system records the full pulse shape using flash ADCs with 1 GS/s sampling rate and 12 bits resolution. A trigger signal from the pulsed proton beam starts the data acquisition, and all trigger signals from each proton pulse are recorded in the raw data for off-line analysis. The preprocessed data including neutron time-of-flight (TOF) and pulse height spectra (PH spectra) of gamma from the $C_6D_6$ detector are extracted from the raw files with the data analysis framework ROOT.[21]

## 3. Data analysis

The neutron capture yield $Y(E_n)$ as a function of the incident neutron energy $E_n$ is determined by

$$C(E_n) - B(E_n) = \Phi(E_n) Y(E_n) \varepsilon_c(E_n), \tag{1}$$

where $C(E_n)$ and $B(E_n)$ are the respective counting spectra measured by the $C_6D_6$ system for the sample and the background. $\varepsilon_c(E_n)$ is the efficiency of the detector system to detect a capture event, and $\Phi(E_n)$ is the neutron incident flux. The determination of neutron energy, the deduction of different background components, the correction of detector efficiency and the determination of incident neutron flux are described in the following sub-sections.

### 3.1. Determination of neutron energy

At Back-n, the kinetic energy of a detected neutron is deduced from the length of the flight path ($L$) and the flight time ($T_n$) of the neutron via the classical formula

$$E_n = \frac{1}{2} m_n \frac{L^2}{T_n{}^2}. \tag{2}$$

Experimentally the flight time $T_n$ is derived from the time difference between the neutron production and the detection of reaction products (the $\gamma$-rays in capture measurement). As the flight time of the so-called $\gamma$-flash which originates from the proton spallation reaction can be accurately determined by the distance ($L_0$) between the outer surface of the spallation target and the front face of the detector, it is usually used as a time reference in TOF measurements. The TOF of each neutron is given by

$$T_n = T_e - T_s + \frac{L_0}{c}, \tag{3}$$

where $T_e$ is the stop signal that represents the moment of the observed time of neutrons, $T_s$ is the start signal which origiantes from the arrival of the $\gamma$-flash at each detector. $L_0/c$ is the time spent of $\gamma$-ray's transport in the vacuum tube. The flight path length $L$ is the sum of the fixed distance $L_0$ and an energy-dependent term $\Delta L$ that results from the neutron moderation process in the spallation target. In this work, $L$ was calibrated by using a measurement of standard resonances of $^{197}$Au and an average length of about 76.69 m was used to calculate the neutron energy.[22] The measurements of the $^{197}$Au$(n,\gamma)$ cross section can be found in the literature.[23,24] For obtaining the experimental counting spectrum, a series of parameters were extracted and analyzed from the digital waveforms of the $C_6D_6$ detectors, i.e., the amplitude, the baseline and signal area.[25]

### 3.2. Background deduction

An accurate evaluation of the backgrounds is of great importance for this work. The dedicated study on background for neutron capture cross section measurements with $C_6D_6$ detectors at Back-n can be found in the literature.[25] Figure 2 shows the experimental counting spectra mesured by different samples, which are all normalized by the counting of a Li–Si monitor detector. Several types of backgrounds contribute to the present measurement, which can be calculated by

$$B(E_n) = B_0 + B_{em}(E_n) + B_s(E_n). \tag{4}$$

The time-independent background $B_0$ mainly comes from the natural environment, the radioactivity of the $^{232}$Th sample and the activation of materials around the detector system. This background has been estimated by a series of measurements with the accelerator shutting down.

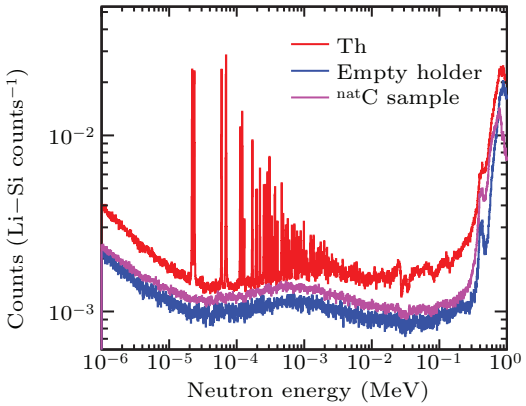



**Fig. 2.** Counting spectrum of $^{232}$Th sample, accompanying with different components of background.

The sample-independent background $B_{\rm em}(E_{\rm n})$ originates from the neutron beam reactions with anything other than the $^{232}$Th sample. Namely, it represents all the effects caused by the neutron beam but not by the sample. This background component is evaluated by a measurement of empty-sample holder with the neutron beam switched on.

Another source of background $B_{\rm s}(E_{\rm n})$ is attributable to the neutrons scattered from samples. Some scattered neutrons would be thermalised and captured by the materials around the detectors. The resulting $\gamma$-rays are recorded by the $C_6D_6$ detectors and will inevitably contaminate the capture yield from the $^{232}$Th sample. This background can be evaluated by a measurement of a natural graphite sample ($^{\rm nat}$C) which has a quite small capture cross section but a considerably high scattering cross section. For calculating the scattering neutron background of thorium, a ratio $\eta$ that represents the difference between the scattered neutrons from the $^{232}$Th sample and the $^{\rm nat}$C sample is calculated by the Geant4 Monte–Carlo simulation.[26] This background component can be expressed as

$$B_{\rm s}(E_{\rm n}) = \eta(N_{\rm C}(E_{\rm n}) - N_{\rm EM}(E_{\rm n})), \tag{5}$$

where $N_{\rm C}(E_{\rm n})$ and $N_{\rm EM}(E_{\rm n})$ represent the experimental spectra of the graphite sample and the empty holder, respectively. Figure 3 shows the ratio $\eta$ as a function of neutron energy, which was obtained by simulating the number of the scattered neutrons entering the detectors from the $^{232}$Th sample and the $^{\rm nat}$C sample.[6,25,27] The ratio $\eta$ is related to the atomic density and the neutron scattering cross section of the samples. And the product of $\eta$ and the experimental spectra of the $^{\rm nat}$C sample were used to evaluate the scattered neutron background of $^{232}$Th. The systematic uncertainty ascribed to the background deduction propagates into the final capture yield according to the signal-to-background ratio. By comparing the TOF spectra measured with the empty holder and the $^{232}$Th sample, an uncertainty of about 1.5%–1.9% was deduced in the URR from 4 keV to 100 keV.[28,29]

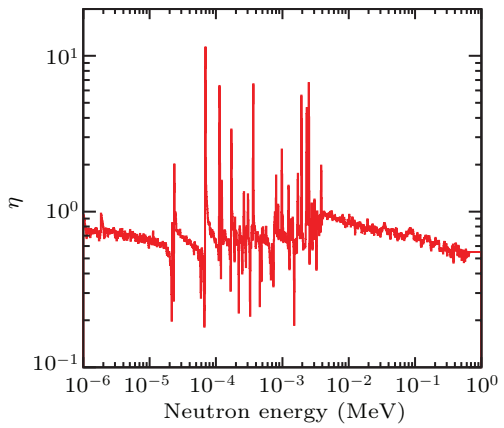



**Fig. 3.** Ratio $\eta$ as a function of neutron energy.

### 3.3. Detector efficiency

The $\gamma$-ray detection from a neutron capture event is related to the de-excitation path of a compound nucleus, which means that the actual count directly observed in the detector system is not equal to the count of capture events expected. Considering the multiplicity of the $\gamma$-ray cascade, the PHWT[17–19] has been applied in the data analysis procedure, which is based on the following two conditions:[19] (1) the efficiency to detect $\gamma$-rays ($\varepsilon_{\gamma i}$) must be low enough to assure that at most only one $\gamma$-ray of a capture cascade is detected at a time. The total efficiency to detect a capture event ($\varepsilon_{\rm c}$) can be approximately calculated by

$$\varepsilon_{\rm c} = 1 - \prod_i (1 - \varepsilon_{\gamma i}) \approx \sum_i \varepsilon_{\gamma i}. \tag{6}$$

(2) $\varepsilon_{\gamma i}$ is proportional to the register $\gamma$-ray energy $E_{\gamma i}$, i.e., $\varepsilon_{\gamma i} = kE_{\gamma i}$. Therefore, the efficiency $\varepsilon_{\rm c}$ becomes

$$\varepsilon_{\rm c} \approx k\sum_i E_{\gamma i} \approx kE_x = k(S_{\rm n} + E_{\rm n,c}), \tag{7}$$

where $E_x$ represents the excitation energy of the compound nucleus system, which equals the sum of neutron binding energy $S_{\rm n}$ and incident neutron kinetic energy $E_{\rm n,c}$. With Eq. (7), the detection efficiency is independent of the details of the $\gamma$-ray cascade path and becomes neutron energy-dependent. Unfortunately, for the $C_6D_6$ detector system, $\varepsilon_{\gamma i}$ is small enough but it is not directly proportional to the $\gamma$-ray energy. Therefore, the correction of the detector efficiency to $\gamma$ ray is indispensable.

The original efficiency to detect a $\gamma$ ray is related to the detector response function $R(E_{\rm d})$ via

$$\varepsilon_{\gamma i} = \int R(E_{\rm d})\,{\rm d}E_{\rm d}, \tag{8}$$

where $E_{\rm d}$ represents the energy deposition in the detectors, and $R(E_{\rm d})$ is the probability distribution of the deposited energy. To achieve the proportionality between the $\gamma$-ray efficiency and the $\gamma$-ray energy, a mathematical manipulation based on Monte–Carlo simulations is used. The detector response functions for different $\gamma$-ray energies are artificially weighted by a proper weighting function (WF), and the $\gamma$-ray efficiency becomes

$$\varepsilon_{\gamma i} = \int R(E_{\rm d}){\rm WF}(E_{\rm d})\,{\rm d}E_{\rm d} = kE_{\gamma i}. \tag{9}$$

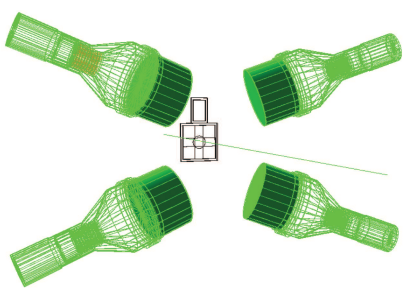


**Fig. 4.** Geometry of the detector system used in Geant4 simulation.

In this work, the WF is determined by simulating the detector response functions of a series of monoenergetic $\gamma$-rays released from the sample using the Monte–Carlo toolkit Geant4.[26] The detailed geometry of the complete experimental set-up including the detectors and sample, displayed in Fig. 4, is taken into account in the simulation. The details on the applications of PHWT and the calculatios of WF for the $C_6D_6$ detector system at the Back-n beam line of CSNS are explained extensively in the literature[20] and references therein.

Figure 5 shows the detector efficiency before (Fig. 5(a)) and after weighting (Fig. 5(b)). The ratio $Q$ (Fig. 5(c)) between the weighted efficiency and $\gamma$-ray energy is usually used to estimate the quality of PHWT. An expected value of 1 for $Q$ at different incident $\gamma$-ray energies shows a great rationality of the weighting function in the energy range of interest. The deviation at low energies is caused by that the threshold of $\gamma$-ray energy used in the simulation is 150 keV, and the detectors are impossible to record valid signals at the low energy due to the experimental limitations.

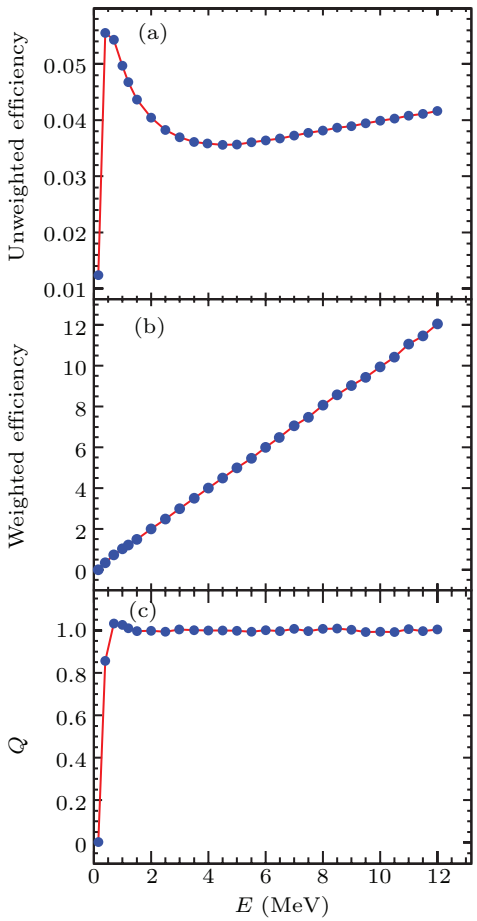



**Fig. 5.** Detector efficiency before (a) and after weighting (b). By the weighting procedure, the ratio between the detector efficiency and $\gamma$-ray energy is equal to 1 (c).

After the correction of the detector efficiency, the experimental capture yield $Y(E_n)$ is calculated via

$$C_w(E_n) - B_w(E_n) = \Phi(E_n)Y(E_n)kE_x, \qquad (10)$$

with $C_w$ and $B_w$ being the weighted count spectra of the sample and the background. The proportionality constant $k$ is taken equal to 1 MeV$^{-1}$. $\Phi(E_n)$ and $E_x$ in Eq. (10) have the same meaning as in Eqs. (1) and (7), respectively. In this way, the experimental neutron capture yield can be calculated without considering the actual cascade path. Several systematic effects related to the PHWT contribute to the final yield, i.e., the efficiency of more than one $\gamma$-ray detected in a capture cascade (see Eq. (1)), the adequacy of the WF used, the reduction of cascade $\gamma$-ray due to the electron internal conversion process, the count loss due to the energy threshold and so on. These effects have been discussed extensively in the literature,[18–20,30] and the systematic uncertainty of the experimental neutron capture yields from the PHWT is about 2%.[18]

### 3.4. Neutron flux and normalization

Although $\Phi(E_n)$ is crucial for the calculation of the capture yield (see Eq. (10)), the absolute value of neutron flux incident on the sample is unknown in the capture cross section measurement. This issue is solved by the so-called saturated resonance technique.[31]

In the previous work, the $^{235}$U/$^{238}$U multi-layer fission ionization chamber (MFC) based on the $^{235}$U (n,f) reaction was used to measure the relative energy dependence of neutron flux (i.e., the source neutron energy spectrum) up to hundreds of MeV.[32] And at neutron energies below 10 keV, the Li–Si neutron monitor based on the detection of $^6$Li(n, t)$^4$He reaction product was applied to measure the flux with less obvious resonance structures.[33] The relative neutron flux (see Fig. 6) adopted for the calculation of capture yield is the pointwise data from the experimental results of these two detectors, with an overall systematic uncertainties about 8% for neutron energies between 4 keV to 100 keV. More details on the neutron energy spectrum evaluation can be found in the literature.[32,33] As shown in Fig. 6, this spectrum is a combination of the measurement results in ES#1 and ES#2, and it is widely used in the capture measurements at Back-n at present. The fluctuation in the measured flux, especially at low energies, is related to the resonance structure of the materials in the neutron beam and the detector.

In the data analysis of $^{232}$Th $(n,\gamma)$ cross section measurement, the absolute normalization of the capture yield is determined by the nearly saturated resonance at $E_n = 23.5$ eV of thorium, with a peak transmission of about 0.3%. At this resonance energy, the macroscopic total cross section is large enough $(n\sigma_t \gg 1)$ to ensure that all incident neutrons can interact with the sample so that the neutron transmission can be negligible. And the neutron width is much smaller than the capture width ($\Gamma_n \ll \Gamma_\gamma$), which ensures that all the incident neutrons in the vicinity of this resonance energy get captured by the sample. Therefore, the neutron capture yield (including

the neutron multiple scattering effect) at the resonance energy is close to unity. To evaluate the systematic uncertainty of the normalization, the experimental data should be fitted using different resonance parameters based on a rigorous theoretical analysis.[7,8] However, in the present work, a systematic uncertainty of about 1% is given for the self-normalization by simply comparing different normalization cofficients obtained by the experimental yield and theoretical yield at the resonance top.[34] This uncertainty is also correlated to the accuracy of the shape of the neutron flux, which will be discussed in detail in the following section.

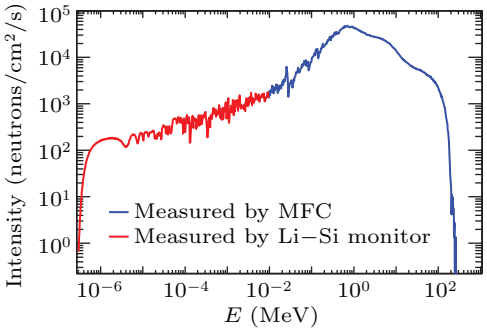



**Fig. 6.** Source neutron spectrum measured by Li–Si monitor detector (red line) and by $^{235}$U/$^{238}$U multi-layer fission ionization chamber (blue line).

## 4. Results and disscussion

### 4.1. Determination of the (n, $\gamma$) cross section

The capture yield $Y(E_n)$ in a capture experiment is related to the capture cross section $\sigma_c$ and the total cross section $\sigma_t$ via the following formula:

$$Y(E_n) = (1 - e^{-Nd\sigma_t(E_n)})\frac{\sigma_c(E_n)}{\sigma_t(E_n)}f_c(E_n), \quad (11)$$

where $N$ is the atomic density of the sample, $d$ is the sample thickness, and the capture yield $Y(E_n)$ is calculated through Eq. (10) which has been described in detail in Section 3. In the (n, $\gamma$) cross section measurement, the correction $u(E_n)$ of neutron multiple scattering and self-shielding effect in the sample must be made for the sample with a finite thickness, which is calculated by

$$u(E_n) = f_c(E_n)\frac{(1 - e^{-Nd\sigma_t(E_n)})}{Nd\sigma_t(E_n)}, \quad (12)$$

where $f_c(E_n)$ is the energy-dependent factor for multiple scattering correction, and the term in the parenthesis of the right side of Eq. (12) accounts for the self-shielding effect. As it is difficult to deduct the contribution of these two effects through experiment, the correction is generally obtained by Monte–Carlo simulations[35] or analytical approaches.[36] In this work, we used again the Geant4 code to calculate the multiple scattering correction $f_c(E_n)$. Combined with the calculation of Eq. (12), the result of the correction factor $u(E_n)$ was obtained and it ranges from about 1.036 to 1.067 for the $^{232}$Th sample from 4 keV to 100 keV. Then, the average capture cross section $\langle\sigma_c(E_n)\rangle$ of $^{232}$Th was derived from the corrected average capture yield $\langle Y(E_n)\rangle$ via

$$\langle Y(E_n)\rangle = u(E_n)Nd\langle\sigma_c(E_n)\rangle. \quad (13)$$

### 4.2. Discussion of results and uncertainties

The results of this work and several experimental data from the previous measurements are plotted in Fig. 7, accompanying with the evaluated data from the Evaluated Nuclear Data File Version B-VIII.0 (ENDF/B-VIII.0),[37] as well as the Chinese Evaluated Nuclear Data Library (CENDL-3.1).[38]

In addition, the $^{232}$Th (n, $\gamma$) reaction cross-sections in the unresolved resonance region from 4 keV to 100 keV were also theoretically studied by using the computer code TALYS-1.95[13] with default parameters. TALYS is an open source software package for prediction and analysis of nuclear reactions. It can calculate the nuclear reactions that involve neutrons, photons, protons, deuterons, tritons, $^3$He- and alpha-particles, in the 1 keV–200 MeV energy range for target nuclides of mass 12 and heavier.[13] The calculation of TALYS is not used as a fitting of the measured result in this work, but as a prediction for nuclear reactions and neutron nuclear cross section in the URR. In this work, all possible exit reaction channels and all associated cross sections of n+$^{232}$Th reaction at different neutron energies were taken into account and the cross section of the $^{232}$Th (n, $\gamma$) reaction was extracted and analyzed. The results of theoretically calculated excitation function are also shown in Fig. 7. All the cross section data are included in the SM and the datasets are openly available at http://dx.doi.org/10.11922/sciencedb.j00113.00015.

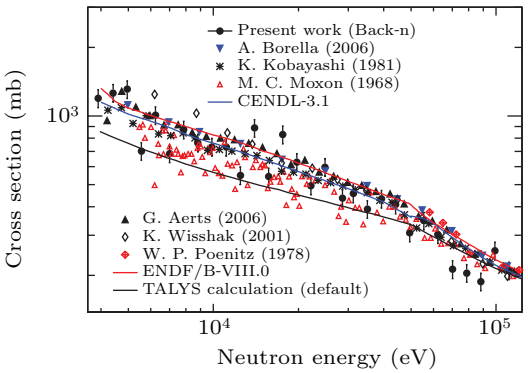



**Fig. 7.** Comparison of the present experimental data, several existing data from EXFOR, the evaluated data from ENDF/B-VIII.0 and CENDL-3.1, and the theoretical calculation data from TALYS. In order to keep the figure readable, the uncertainties for the existing experimental data are omitted.

As presented in Fig. 7, it can be seen that the trend of the present measurement data is consistent with the theoretical calculation results from TALYS and the evaluated data of ENDF/B VIII.0[37] and CENDL-3.1[38] in the URR from 4 keV to 100 keV. The theoretical cross sections calculated by TALYS using the default parameters are slightly lower than the

evaluated data. Although the neuton energy region at Back-n is expanded to tens of MeV, the results here are limited to about 100 keV because the system uncertainties increase significantly at higher energy. Compared with the data measured by Aerts *et al.*[5] at n_TOF and by Broella *et al.*[8] at GELINA, the present measured data shows a greater deviation and fluctuation with the evaluated data. The structures of the neutron spectrum cannot be excluded as an important contribution to the fluctuation since these are greater than those in the thorium data. The similar fluctuations also exist in the measurements of other samples.[23,24] Another important reason for the discrepancy between our data and the existing data is the different normalization procedures. In the present measurement, the capture yield is normalized by a saturated resonance at the low neutron energy so that the structure of the energy spectrum at around this energy will inevitably disturb the accuracy of normalization. It is worth considering a new specialized measurement of the source neutron spectrum to offer more accurate data in the future. However, it is hard for us at present to evaluate the systematic uncertainty of normalization which is combined with the shape of the neutron flux. In addition, the new capture experiments of other isotopes recently performed at Back-n have indicated that the in-beam $\gamma$ background resulted from the neutron captures on hydrogen in the spallation target assembly may lead to the discrepancy of experimental cross section, which is worth exploring in our newly planned measurement.

The uncertainty of the present measurement originates from several components, including the statistical and systematic uncertainties. The statistical uncertainties are evaluated by the formula of $N^{-0.5}$ for $N$ events in an energy bin. Thanks to the high neutron flux and the adequate measurement time provided by Back-n, the statistical uncertainties in the URR are less than 1%. The contributions of systematic uncertainties can be inferred from the experimental data analysis procedure and have been described in Section 3. These components are listed in Table 2. It can be concluded that the systematic uncertainty related to the energy dependence of the neutron flux plays a dominant role in the URR. The total uncertainties are shown in Fig. 7 in the form of error bars on the measured cross sections.

**Table 2.** System uncertainties in the measured capture cross section.

| Contributions | Uncertainty |
|---|---|
| PHWT | 2.0% |
| Neutron flux shape | 8.0% |
| Background subtraction | 1.5%–1.9% |
| Normalization | 1.0% |

### 4.3. Average parameters

In the unresolved resonance region, the cross section is parameterized by the statistical models. Fictitious resonances are generated to characterize the average cross section, which is a substantially different way to describe the cross section in the RRR, with a set of individual resonance parameters for each resonance peak. The fictitious resonances described by the average parameters enable the calculation of cross section, which are essential for the neutron transport calculations of reactors. Hence, it is crucial to extract and analyze the average parameters from the measured cross section.

In the URR, the average cross section $\langle\sigma_{cc'}\rangle$ for a neutron-induced reaction from the entrance channel $c$ to the exit channel $c'$ can be expressed as

$$\langle\sigma_{cc'}\rangle = \pi\lambda_c^2 g_c\langle(\delta_{cc'} - U_{cc'})\rangle, \tag{14}$$

where $U_{cc'}$ are the average collision matrixes and they are related to $R$ matrix through some intermediate parameters. The main parameters for the determination of capture cross section in URR include the mean level spacing $D_l$, the neutron strength function $S_l$, the average radiation width $\langle\Gamma_\gamma\rangle_l$, and the effective scattering radius $R'$. The subscript $l$ is the orbital angular momentum of the incident channel.

The code FITACS, which has been integrated into SAMMY-M5,[36] was used to fit the capture cross section based on the Hauser–Feshbach theory with width fluctuations. In this code, the energy dependence of the radiation widths is specified via the giant dipole model, and of the mean level spacing for s-waves via the Gilbert–Cameron composite formula. The mean spacings for $l > 0$ are given via the Bethe formula and Moldauer prescription is used for partial cross sections.[36] Generally, a simultaneous fit including the data sets of different types of reaction cross sections is recommend to determine the average resonance parameters. In this work, we used only the present capture data. In order to obtain realistic results, the initial values of the varied parameters should not diverge outside of the constraints of the theory. The starting values of neutron strength functions for s-wave ($S_0 = 0.87\times10^{-4}$) and p-wave ($S_1 = 1.90\times10^{-4}$) are taken from the literature,[39] and that for d-wave ($S_2 = 0.89\times10^{-4}$) is adopted from the literature.[5] The average radiation width $\langle\Gamma_\gamma\rangle_l$ for $l = 0$–2 and the mean level spacing for $l = 0$ ($D_0 = 17.2$ eV) are also obtained from the literature.[5] In addition, the distant-level parameter $R^\infty$ is obtained via $R^\infty = 1 - R'/a$, where $R'$ is the effective scattering radius and $a$ represents the channel radius with the units of Fermi. For the effective scattering radius, we obtain value $R' = 9.65$ fm from the Atlas of Neutron Resonance.[40] And the channel radius $a$ is calculated through $a = 1.23([A/m_n]^{1/3} + 0.8)$. Finally, the related initial value of s-wave distant-level parameter $R^\infty$ is $-0.13$.

Other fixed input parameters such as the neutron binding energy, the pairing energy, the center-of-mass excitation energy, spin, and parity for different target levels are adopted from the Evaluated Nuclear Structure Data File (ENSDF) of the National Nuclear Data Center (NNDC). The final fitted results are shown in Fig. 8. The strength functions for s-wave

and p-wave resonances are both fixed during the fitting. The fitting parameter results are $S_2 = 1.15 \times 10^{-4}$, $\langle \Gamma_\gamma \rangle_0 = \langle \Gamma_\gamma \rangle_2 = 23.9$ meV, and $\langle \Gamma_\gamma \rangle_1 = 25.8$ meV.

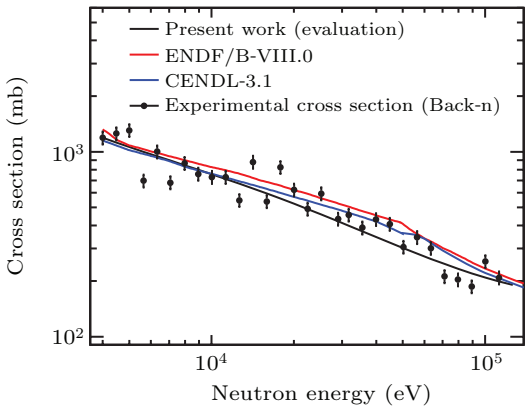



**Fig. 8.** Experimental cross section and the result of evaluation.

## 5. Conclusion

The $^{232}$Th neutron capture reaction cross section has been measured at the Back-n facility of CSNS using the $C_6D_6$ liquid scintillation detectors for the first time. A detailed description of the data analysis procedure and the system uncertainty evaluation was given. The $^{232}$Th $(n, \gamma)$ cross section data in the unresolved resonance region from 4 keV to 100 keV were compared with the code TALYS, several existing data from previous measurements, the data from ENDF/B-VIII.0 and CENDL-3.1 evaluation database and were found in consensus. The average parameters in the unresolved resonance region were also obtained by using the code FITACS to fit the experimental cross section and that generated via the theory. The present measurement could offer an important reference for the experimental design of neutron capture cross section measurement at the Back-n facility. Further measurements will be prepared to mitigate the fluctuation and improve the accuracy of experimental cross section.

## Data availability

The data that support the findings of this study are openly available in Science Data Bank at http://dx.doi.org/10.11922/sciencedb.j00113.00015.

## Acknowledgements

The authors would like to thank the Back-n collaboration for discussions.

Project supported by the Chinese TMSR Strategic Pioneer Science and Technology Project (Grant No. XDA02010000) and the National Natural Science Foundation of China (Grant No. 11790321).

## References

[1] Cai X Z, Dai Z M and Xu H J 2016 *Physics* **45** 578 (in Chinese)
[2] Jiang M H, Xu H J and Dai Z M 2012 *Bull. Chin. Acad. Sci.* **27** 366 (in Chinese)
[3] Bowman C D, Arthur E D, Lisowski P W, *et al*. 1992 *Nucl. Instr. Meth. A* **320** 336
[4] Hu J F, Wang X H, Wu J H, Cai X Z, Han J L and Chen J G 2018 *At. Energy Sci. Technol.* **52** 1206 (in Chinese)
[5] Aerts G, Abbondanno U, Álvarez P H, *et al*. 2006 *Phys. Rev. C* **73** 054610
[6] Gunsing F, Berthoumieux E, Aerts G, *et al*. 2012 *Phys. Rev. C* **85** 064601
[7] Lobo G, Corvi F, Schillebeeckx P, Janeva N, Brusegan A and Mutti P 2002 *J. Nucl. Sci. Technol.* **39** 429
[8] Borella A, Volev K, Brusegan A, Schillebeeckx P, Corvi F, Koyumdjieva N, Janeva N and Lukyanov A A 2006 *Nucl. Sci. Eng.* **152** 1
[9] Tang J Y, Jing H T, Xia H H, Tang H Q, Zhang C, Zhou Z Y, Ruan X C, Zhang Q W and Yang Z 2013 *At. Energy Sci. Technol.* **47** 1089 (in Chinese)
[10] Tang J Y, An Q, Bai J B, *et al*. 2021 *Nucl. Sci. Tech.* **32** 1
[11] Wei J, Chen H S, Chen Y W, *et al*. 2009 *Nucl. Instr. Meth. A* **600** 10
[12] Chen H S and Wang X L 2016 *Nat. Mater.* **15** 689
[13] Koning A J and Rochman D 2012 *Nucl. Data Sheets* **113** 2841
[14] Zhang L Y, Jing H T, Tang J Y, Li Q, Ruan X C, Ren J, Ning C J, Yu Y J, Tan Z X, Wang P C, He Y C and Wang X Q 2018 *Appl. Radiat. Isot.* **132** 212
[15] Jiang B, Han J L, Jiang W, Hu J F, Wang X H, Chen J G and Cai X Z 2021 *Nucl. Instr. Meth. A* **1013** 165677
[16] Jing H T, Tang J Y, Tang H Q, Xia H H, Liang T J, Zhou Z Y, Zhong Q P and Ruan X C 2010 *Nucl. Instr. Meth. A* **621** 91
[17] Macklin R L and Gibbons J H 1967 *Phys. Rev.* **159** 1007
[18] Abbondanno U, Aerts G, Alvarez H, *et al*. 2004 *Nucl. Instr. Meth. A* **521** 454
[19] Borella A, Aerts G, Gunsing F, Moxon M, Schillebeeckx P and Wynants R 2007 *Nucl. Instr. Meth. A* **577** 626
[20] Ren J, Ruan X C, Bao J, *et al*. 2019 *Radiat. Detec. Technol. Meth.* **3** 1
[21] Antcheva I, Ballintijn M, Bellenot B, *et al*. 2009 *Comput. Phys. Commun* **180** 2499
[22] Ren J, Ruan X C, Jiang W, *et al*. 2021 *Chin. Phys. C* (Accepted)
[23] Li X X, Liu L X, Jiang W, *et al*. 2020 *Nucl. Tech.* **43** 86 (in Chinese)
[24] Hu X R, Fan G T, Jiang W, *et al*. 2021 *Nucl. Sci. Tech.* **32** 1
[25] Ren J, Ruan X C, Jiang W, *et al*.2021 *Nucl. Instr. Meth. A* **985** 164703
[26] Agostinelli S, Allison J, Amako K, *et al*. 2003 *Nucl. Instr. Meth. A* **506** 250
[27] Massimi C, Domingo-Pardo C, Vannini G, *et al*. 2010 *Phys. Rev. C* **81** 044616
[28] Lederer C, Massimi C, Berthoumieux E, *et al*. 2014 *Phys. Rev. C* **89** 025810
[29] Mastromarco M, Manna A, Aberle O, *et al*. 2019 *Eur. Phys. J. A* **55** 1
[30] Tain J L, Gunsing F, Aniel-Cano D, *et al*. 2002 *J. Nucl. Sci. Technol.* **39** 689
[31] Macklin R L, Halperin J and Winters R R 1979 *Nucl. Instr. Meth.* **164** 213
[32] Chen Y H, Luan G Y, Bao J, *et al*. 2019 *Eur. Phys. J. A* **55** 1
[33] Li Q, Luan G, Bao J, *et al*. 2019 *Nucl. Instr. Meth. A* **946** 162497
[34] Li X X, Liu L X, Jiang W, *et al*. 2021 *Phys. Rev. C* **104** 054302
[35] Larson N M and Volev K N 2002 *PHYSOR 2002*, October 7–10, 2002, Seoul, Korea
[36] Larson N M 2000 *Technical Report, ORNL/TM-9179 R5*, Oak Ridge National Laboratory, Oak Ridge, TN, USA
[37] Brown D A, Chadwick M B and Capote R 2018 *Nucl. Data Sheets* **148** 1
[38] Ge Z G, Zhao Z X, Xia H H, Zhuang Y X, Liu T J, Zhang J S and Wu H C 2011 *J. Korean Phys. Soc* **59** 1052
[39] Soukhovitskii E S, Capote R, Quesada J M and Chiba S 2005 *Phys. Rev. C* **72** 024604
[40] Rowlands J 2006 *Ann. Nucl. Energy* **33** 1157